Laser-induced short- and long-range orderings of Co nanoparticles on SiO_2

C. Favazza, J. Trice, H. Krishna, and R. Kalyanaraman[a)]
Department of Physics, Washington University in St. Louis, Missouri 63130
and Center for Materials Innovation, Washington University in St. Louis, Missouri 63130

R. Sureshkumar
Department of Chemical Engineering, Washington University in St. Louis, Missouri 63130

(Received 30 November 2005; accepted 16 March 2006; published online 12 April 2006)

Laser irradiation of ultrathin Co films leads to pattern formation by dewetting with short-range order (SRO) as well as long-range order (LRO). When a 1.5 nm thick Co film is irradiated by a single laser beam, a monomodal size distribution of particles with average diameter of 31 ± 10 nm and nearest-neighbor spacing of 75 nm is observed. Moreover, melting by two-beam interference irradiation produces LRO as well as SRO giving a *quasi-two-dimensional* arrangement of nanoparticles. The SRO is attributed to spinodal dewetting while the LRO is conjectured to be induced by in-plane interfacial tension gradients. Laser-induced dewetting of metals could be a simple technique to fabricate ordered metal nanoarrays. © *2006 American Institute of Physics*. [DOI: 10.1063/1.2195113]

Metal nanoarrays comprising nanoparticles have many applications including, in surface plasmon waveguides made from linear chains of metal nanoclusters,[1,2] in arrays of discrete nanometer scale magnetic alloys as memory storage devices[3] and as catalyst arrays for the growth of carbon nanotubes.[4] However, the assembly of metal nanostructures with order poses several challenges, including limitations on controlling the particle size and spacing at length scales below the diffraction limit. One potentially simple process of pattern formation with spatial order is through dewetting, as has been observed with polymer films.[5,6] In general, two routes are proposed for pattern evolution via dewetting: one by homogeneous nucleation and growth of the holes and the other by a pattern forming hydrothermal instability.[7,8] One important distinction between these two dewetting routes is that the instability is usually associated with a characteristic length scale. There have been few exhaustive studies on dewetting of ultrathin metal films from inert substrates with the goal of making ordered nanostructures. One reason for this is the high melting point of most metals, making dewetting by solid-state diffusion a slow process even at high temperatures. Pulsed laser heating has been used in the past to investigate dewetting in metals.[7,9] The rapid heating rates and finite melt lifetimes following pulsed laser melting have permitted investigation of dewetting in various metals, such as Au, Cu, and Ni. We have recently observed that pulsed laser irradiation of Co shows evidence for dewetting and nanoparticle formation on an SiO_2 surface (unpublished). Here we show that single beam and two-beam UV laser irradiations of Co films lead to nanoparticle morphologies with well-defined length scales. Two-beam interference irradiation of the metal film produces long-range order (LRO) with a length scale identical to the interference spacing as well as short-range order (SRO) in a direction perpendicular to the laser fringes. The LRO is attributed to potential mass transport induced by interfacial tension gradient generated by the spatially nonuniform temperature field while the SRO is attributed to the spinodal dewetting instability. Understanding this laser-induced dewetting phenomenon in metals could have significant implications towards developing a simple laser-processing approach to manufacture metal nanoclusters with a large degree of ordering.

Co films of either 1.5 or 2.5 nm thickness were deposited onto multiple pieces of SiO_2/Si wafers by e-beam evaporation at room temperature (RT). The oxide layer thickness was 400 nm. The specific details of the deposition geometry have been published elsewhere.[10,11] The deposition rate used here was 1 nm/min. The chamber pressure prior to deposition was $\sim 2 \times 10^{-8}$ Torr and during deposition was $\sim 3.5 \times 10^{-8}$ Torr. The wafers were degreased in acetone, methanol, and de-ionized (DI) water prior to film deposition.

Following the deposition of Co onto the substrates, laser processing was performed by one of two ways: (1) the 1.5 nm Co film was laser irradiated for 600 pulses by a single beam incident perpendicular to the Co film and (2) two-beam irradiation at an interference angle of 49° was performed on the 2.5 nm film for 600 shots. This angle gives a theoretical fringe spacing of 321 nm. The laser beam energy density used for the one-beam irradiation was 120 ± 10 mJ/cm^2. For the two-beam case a primary beam of energy 120 mJ/cm^2 was split into two beams with resulting intensity contrast on the sample of 30%. The laser used was a spectra physics injection seeded Lab-130-50 Nd:YAG (yttrium aluminum garnet) laser operating at its fourth harmonic of 266 nm, with a pulse width $\tau_p \sim 9$ ns and repetition rate $f = 50$ Hz. The pattern formation was investigated in an approximately 50×100 μm^2 region of the laser beam within which the energy density variation was 20% in each of the two dimensions. The laser energy density was chosen to produce a detectable change in film morphology within a few pulses. We determined that a sharp energy threshold exists below which no substantial morphology change can be detected. This effect has previously been correlated with the melt threshold of the films.[12] Numerical modeling via finite element analysis using the program FEMLAB showed that chosen energies were close to the melt threshold energy for the respective film thicknesses. The resulting film morphology was characterized using scanning electron microscopy (SEM) in a Hitachi S-4500 microscope.

Figure 1(a) is a SEM micrograph showing that the 1.5 nm Co film consists of a particulate morphology follow-

a)Electronic mail: ramkik@wustl.edu

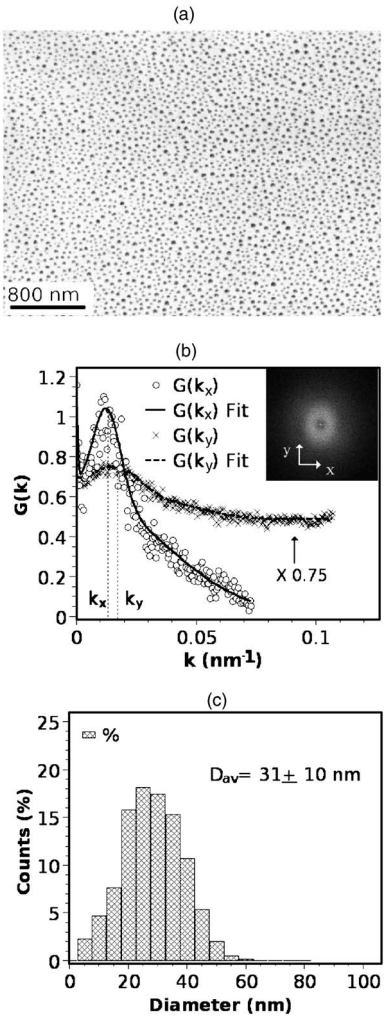

FIG. 1. (a) Nanoparticle morphology of 1.5 nm thick Co film following single-beam laser irradiation; (b) power spectrum (inset) of (a) showing evidence for SRO in the form of the broad bright ring. The RDF's in x and y were used to identify the SRO peak position with least-squares fitting; (b) the particle size histogram showing a monomodal size distribution with an average diameter of 31 ± 10 nm.

ing single beam laser irradiation. To analyze the spatial ordering among the nanoparticles, the power spectrum was calculated and is shown in the inset of Fig. 1(b). The power spectrum is a distinct ring with asymmetry in the x and y directions. This ring is evidence for SRO as can be seen from the analysis of the radial distribution function (RDF) $G(k)$ in the x and y directions plotted in Fig. 1(b). $G(k)$ shows broad but distinct peaks in the two directions. The peak positions (marked in the figure) were identified by least-squares fitting using Gaussian peak shapes and were determined to be at spatial length scales of $R_x = 85$ nm and $R_y = 65$ nm. We define the mean spacing as the average of these two spacings, which is 75 nm. These length scales correspond to the average nearest-neighbor (NN) spacing between the Co nanoparticles in the x and y directions, respectively. Figure 1(c) is the histogram of particle size showing a broad but monomodal distribution with an average diameter of 31 nm and a standard deviation of 10 nm.

We verified that the pattern formation is due primarily to mass transport of Co on the surface rather than evaporation during the laser heating. This was determined by comparing the total Co concentration before and after laser heating by energy dispersive x-ray spectrometry (EDS) in the SEM. EDS showed that the concentration difference was within the measurement error of 10%. Further, we also verified that chemical interaction between the Co and SiO_2 was minimal by using a preferential metal etch[13,14] to remove the Co. Subsequent measurement using EDS showed that Co was below detectable limits ($\sim$0.2 nm) indicating that any reaction was minimal.

We believe that the nanoparticles form by dewetting of the molten Co from the SiO_2 surface. Dewetting is energetically favorable whenever the liquid has a finite contact angle with the surface.[15] The contact angle of Co on SiO_2 was estimated by using the average particle diameter of 75 ± 23 nm and the average height of 45 ± 7 nm (measured via an atomic force microscope). By assuming a spherical shape these values resulted in a contact angle of $100° \pm 26°$, which favors the formation of particles. This contact angle is consistent with the generally high values for metals on SiO_2 in vacuum.[16]

The second important property in Fig. 1(a) is the SRO in particle arrangement. This points to dewetting with a characteristic length scale implying a spinodal dewetting instability.[15] As has been discussed previously by various groups, an important difference between homogeneous nucleation and spinodal dewetting is the spatial order.[8,17–20] In principle, heterogeneous nucleation can also lead to nonstochastic distributions in the spacing, especially if the surface has ordered nucleation sites.[21] But, we rule this effect out based on the fact that no preferential nucleation sites are expected on the chemically inert and smooth oxide surface.

Figure 2(a) is an SEM micrograph showing the morphology of the 2.5 nm Co film following two-beam laser interference irradiation. The striking feature is the arrangement of particles along definite rows. These particle rows give rise to sharp diffraction spots in the power spectrum, shown in the inset of Fig. 2(b). The spot spacing corresponds to a real space length scale of 315 nm, which is very close to the theoretical fringe spacing value of 320 nm. Tentatively, this long-range order is attributed partly to thermocapillary effects resulting from the surface tension gradients in the molten liquid. This effect has been well studied in the area of laser surface melting, but over much larger length scales.[22] Preliminary modeling shows that the thermal gradients in the liquid Co can be as large as 0.5 K/nm for the fringe spacings used here, which in turn gives rise to a substantial surface tension gradient.[23]

However, it is not clear whether the thermocapillary effect is the dominant mechanism (e.g., as in the case of hydrothermal Marangoni flows which occur when the Marangoni number, that signifies the relative magnitude of surface tension gradient forces as compared to viscous ones, exceeds a critical value[24]) or it acts to augment the classical spinodal dewetting phenomenon observed for films with uniform temperature. In other words, spinodal dewetting refers to the enhancement of spontaneous curvature fluctuations in thin films by long-range attractive intermolecular forces. For an incompressible fluid under isothermal conditions, the rate of volume change by height fluctuations has to be balanced by mass fluxes by fluid flow, caused as a result of Laplace pressure (which is proportional to the interfacial tension and film curvature) and a contribution to pressure from intermolecular forces. In presence of in-plane thermal gradients, the Laplace pressure itself can be modified since interfacial tension varies along the film over a length scale of the interfer-

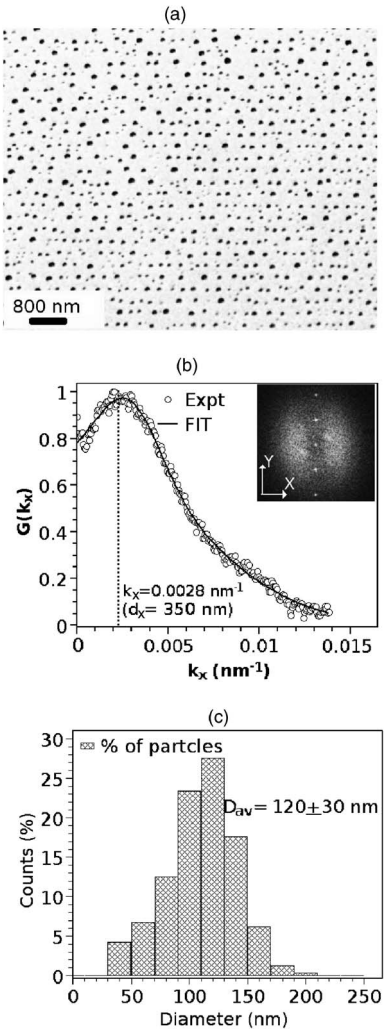

FIG. 2. (a) Nanoparticle morphology of 2.5 nm thick Co film following two-beam interference irradiation showing rows of particles; (b) power spectrum (inset) of (a) showing evidence for LRO in the form of diffraction spots and SRO in the form of the arcs. Also shown is the RDF and fit in the x direction to determine the peak position; (c) the particle size histogram showing a monomodal size distribution with an average diameter of 120±30 nm.

ence wavelength, leading to additional contributions to the mass flux due to flow. Hence, identification of the precise role of thermal gradients on pattern selection requires investigations similar to those reported here under different processes and film parameters.

Another striking result observed in Fig. 2(b) is the distinct arcs in the power spectrum in directions perpendicular to the diffraction spots. The RDF in this direction is plotted in Fig. 2(b) and a broad peak centered around 350 nm is visible. This is again evidence for SRO in the particle arrangement in a direction not constrained by the laser interference fringes. An important consequence of this SRO along the particle rows is that now a *quasi-two-dimensional* (2D) symmetry in particle arrangement is observed despite the one-dimensional (1D) symmetry of the interference pattern. Once again the histogram of particle size distribution [Fig. 2(c)] is monomodal with an average diameter of 120 nm and a standard deviation of 30 nm.

The appearance of the SRO under this spatially nonuniform two-beam laser interference irradiation implies that the instability is not related to the nature of the laser beam uniformity. One puzzling aspect of the result in Fig. 1(b) is the asymmetry observed in the SRO. From the spinodal dewetting instability theory proposed by Vrij,[15] the characteristic length scale for a two-dimensional system, like a thin film, is actually composed of two orthogonal wave vectors, not necessarily equal. Therefore asymmetry in pattern formation is not ruled out in such 2D systems. Nevertheless, future work will aim to resolve this issue.

In conclusion, we have shown that when ultrathin Co films are laser irradiated, Co nanoparticles form by dewetting. The particles have a monomodal size distribution and spatial SRO when formed by a single beam. The SRO is attributed to spinodal dewetting. For two-beam irradiation, both long- and short-range orders are visible, giving rise to a quasi-2D symmetry in particle arrangement. The LRO is conjectured to be caused by contributions to mass transport arising from thermally induced interfacial gradients. These results suggest that understanding pattern formation by laser melting of ultrathin metal films could lead to a simple process for metal nanoarray fabrication.

One of the authors (R.K.) acknowledges support by the National Science Foundation through a CAREER Grant No. DMI-0449258 and to the center for materials innovation for student support.

[1] M. Quinten, A. Leitner, J. Krenn, and F. Aussenegg, Opt. Lett. **23**, 1331 (1998).
[2] S. Maier, P. Kik, H. Atwater, S. Meltzer, E. Harel, B. Koel, and A. Requicha, Nat. Mater. **2**, 229 (2003).
[3] J. Lodder, M. Haast, and L. Abelman, in *Proceedings of NATO Advanced Study Institute on Magnetic Systems Beyond 2000*, Dordrecht, Netherlands, edited by G. C. Hadjipannayis (Kluwer Academic, Dordrecht, 2002), pp. 117–145.
[4] S. Fan, M. Chapline, N. Franklin, T. Tombler, A. Cassell, and H. Dai, Science **283**, 512 (1999).
[5] G. Reiter, Phys. Rev. Lett. **68**, 75 (1992).
[6] P.-G. de Gennes, F. Brochard-Wyart, and D. Quere, *Capillarity and Wetting Phenomenon* (Springer, New York, 2003).
[7] J. Bischof, D. Scherer, S. Herminghaus, and P. Leiderer, Phys. Rev. Lett. **77**, 1536 (1996).
[8] U. Thiele, M. Mertig, and W. Pompe, Phys. Rev. Lett. **80**, 2869 (1998).
[9] J. Bischof, M. Reinmuth, J. Boneberg, S. Herminghaus, T. Palberg, and P. Leiderer, Proc. SPIE **2777**, 119 (1996).
[10] C. Zhang and R. Kalyanaraman, Appl. Phys. Lett. **83**, 4827 (2003).
[11] W. Zhang, C. Zhang, and R. Kalyanaraman, J. Vac. Sci. Technol. B **23**, L5 (2005).
[12] E. Matthias, M. Reichling, J. Siegel, O. W. Kading, S. Petzoldt, H. Skurk, P. Bizenberger, and E. Neske, Appl. Phys. A: Solids Surf. **58**, 129 (1994).
[13] R. Pretorius, J. Harris, and M.-A. Nicolet, Solid-State Electron. **21**, 667 (1978).
[14] L. H. Ho, T. Nguyen, J. C. Chang, B. Machesney, and P. Geiss, J. Mater. Res. **8**, 467 (1993).
[15] A. Vrij, Discuss. Faraday Soc. **42**, 23 (1966).
[16] G. Samsonov, *The Oxide Handbook* (Plenum, New York, 1973).
[17] F. Brochard Wyart and J. Daillant, Can. J. Phys. **68**, 1084 (1990).
[18] A. Sharma, Langmuir **9**, 861 (1993).
[19] S. Herminghaus, K. Jacobs, K. Mecke, J. Bischof, A. Fery, M. Ibn-Elhaj, and S. Schlagowski, Science **282**, 916 (1998).
[20] R. Seemann, S. Herminghaus, and K. Jacobs, Phys. Rev. Lett. **86**, 5534 (2001).
[21] R. Magan, B. Lin, and R. Sureshkumar, J. Phys. Chem. B **107**, 10513 (2003).
[22] D. Bäuerle, Laser Processing and Chemistry (Springer, Berlin, 1996).
[23] T. Anthony and H. Cline, J. Appl. Phys. **48**, 3888 (1977).
[24] E. Guyon, J.-P. Hulin, L. Petit, and C. D. Mitescu, *Physical Hydrodynamics* (Oxford University Press, Oxford, 2001), pp. 439–489.